MEASURING BEDLOAD TRANSPORT RATES BY GRAIN-SIZE FRACTION USING THE SWISS PLATE GEOPHONE SIGNAL AT THE ERLENBACH

Carlos R. Wyss [1, 3],

Dieter Rickenmann [1],

Bruno Fritschi [1],

Jens M. Turowski [1, 2],

Volker Weitbrecht [3],

Robert M. Boes [3].

ABSTRACT

The Swiss plate geophone system is a bedload surrogate monitoring technique that is used to quantify bedload transport in steep streams. The amplitude of the signal recorded by the Swiss plate geophone contains information about the grain-size distribution of the transported bedload. To extract this information, we computed the number of impulses and packets (representing a single particle impact) registered for different amplitude ranges (the so-called *amplitude histograms*) for 46 samples when bedload was measured independently with automatic basket samplers at the Erlenbach. *Amplitude histograms* can be interpreted as a statistical distribution of the signal's amplitude over a given time interval. Using the number of bedload particles per unit mass, we are able to calculate absolute bedload masses for each grain-size class. The results show that the grain-size distribution of the transported bedload for particles larger than 9.5 mm can be continuously monitored at the Erlenbach with the Swiss plate geophone system.

Keywords: Swiss plate geophone, grain-size distribution, amplitude histograms, bedload

[1]Swiss Federal Research Institute WSL, Birmensdorf, Switzerland. E-mail: carlos.wyss@wsl.ch.
[2]Helmholz Centre Potsdam, GFZ German Research Centre for Geosciences, Potsdam, Germany.
[3]Laboratory of Hydraulics, Hydrology and Glaciology VAW, ETH Zürich, Zürich, Switzerland.

19 transport, indirect measurement.

INTRODUCTION

Bedload transport affects any construction work in or near flowing water. In addition, it is an important natural hazard responsible for considerable financial damage especially in alpine regions (Badoux et al. 2014). Bedload transport modelling is crucial for engineering planning and for hazard assessment and mitigation. To validate new models for bedload transport calculations in steep streams, it is necessary to measure bedload transport at different discharge conditions. The prospects of obtaining continuous records of bedload transport rates and the potentially low costs related to indirect measurements are the main motivations to develop bedload surrogate monitoring techniques (Bänziger and Burch 1990; Bunte 1996; Rickenmann and McArdell 2007; Gray et al. 2010).

Surrogate bedload monitoring techniques do not directly capture bedload particles moving along the stream bed, like volume changes determined by topographic surveys and ambient seismic monitoring (Gray et al. 2010). An impact structure-like bedload surrogate device consists of a sensor installed on an impact structure against which bedload particles collide when they are transported along the stream bed. The sensor samples the vibrations triggered by the impacting particles. The sampling rate is technique-dependent and varies between a few hundred Hertz for seismic sensors, 10 kHz for the Swiss plate geophone (Rickenmann et al. 2012) and 500 kHz for the hydrophone (Geay 2013).

The complete signal recorded by bedload surrogate monitoring instrument contains a lot of different information and is difficult to analyse (Krein et al. 2008). To interpret the produced signal, summary values like its acoustic energy (Geay 2013), centroid frequency (Thorne 1986), integral, squared integral, maximum amplitude and number of impulses, i.e., the number of times the signal exceeds a pre-defined threshold (Rickenmann et al. 2014) have been employed. The summary values are used to calibrate the bedload surrogate monitoring technique with direct bedload measurements. Calibration is achieved if a significant correlation can be established between a signal summary value and a bedload transport parameter, like its mass or the transport rate Q_s. Accurate bedload data obtained from direct bed-

load sampling is therefore necessary for the calibration. Due to differences in the hydraulic conditions between bedload monitoring sites and in bedload material characteristics, specific in-situ calibration appears to be necessary. The measurements obtained with bedload surrogate techniques are only as good as their calibration (Gray et al. 2010; Turowski and Rickenmann 2011).

In Switzerland, the Swiss plate geophone system has been used for more than a decade to monitor bedload. It has been installed in several mountain streams and has proven to be a robust device for monitoring bedload transport (Rickenmann et al. 2012; Rickenmann et al. 2014). At the Erlenbach stream in Switzerland, the Swiss plate geophone was calibrated with direct bedload samples taken with automatic basket samplers (Rickenmann et al. 2012), where the total number of impulses registered over a certain threshold value correlates well with total transported bedload mass.

Previous studies have demonstrated that the frequency of the signal produced by surrogate bedload monitoring devices is inversely proportional to the size of the colliding particle (Etter 1996; Bogen and Møen 2003; Møen et al. 2010). A similar particle-size-frequency relationship was noticed by Thorne (1986) and Belleudy et al. (2010) when analyzing the self-generating noise created by natural particles.

All methods developed to extract grain size distribution (GSD) information proposed in the literature are frequency-based methods (Barrière et al. 2014; Belleudy et al. 2010; Bogen and Møen 2003; Etter 1996; Møen et al. 2010; Thorne 1986). This implies that the frequency spectrum is computed from the raw signal and some summary value of it, like the spectral centroid or the dominant frequency (Barrière et al. 2014), is correlated with the size of the colliding particles.

Nevertheless, for the Swiss plate geophone system it has already been shown that the amplitude of the signal contains some information on grain sizes (Rickenmann et al. 2014). In this study, we demonstrate that a simple amplitude-based method is able to produce accurate GSD measurements of the bedload material transported over the Swiss plate geophone at

the Erlenbach. The method is based on a statistical distribution of the amplitude of the signal, i.e. amplitude histograms, which are related to the statistical distribution of the transported bedload material (its GSD). The number of transported particles in different grain-size fractions are used as calibration parameter between the amplitude histograms and the GSD of the transported material.

The method for extracting grain size distribution from the Swiss plate geophone that we presented in this paper is compared with the measured bedload fractions of 46 bedload samples collected by the basket samplers at the Erlenbach between 2010 and 2012 during 28 different discharge events.

FIELD MEASUREMENTS AT THE ERLENBACH

The Erlenbach is a steep stream with an average gradient of 18 % located in the Alptal valley in canton Schwyz, Switzerland. Its catchment is located in a Flysch zone and has an area of 0.7 km^2 (Rickenmann 1997; Schuerch et al. 2006). Sliding and creeping slopes result in high sediment supply to the Erlenbach, where in average, 20 bedload transport events occur every year (Rickenmann et al. 2012). Discharge at the Erlenbach is induced by both snowmelt in the spring and high intensity sporadic summer storms. For a complete overview of the observation site, featuring all measuring facilities, see Beer et al. (2014).

Discharge and mean flow velocity measurements

Discharge is measured every minute at a control cross-section 35 m upstream of the Swiss plate geophones. The mean discharge measured at the Erlenbach during the geophone calibration measurements $Q_{\mathrm{mean}} = 589\ \mathrm{l \cdot s^{-1}}$, and it ranged from 203 to 1321 $\mathrm{l \cdot s^{-1}}$.

A recently installed 2D rotating laser sensor TiM551 (SICK 2014) over the Swiss plate geophones continuously monitors the water surface over the cross-section. The laser measures 15 times per second, giving a distance value for each rotational degree (limited to 270°). We recorded the median value of all distance measurements within the same minute for which discharge is measured. The laser detects the surface only if turbidity is high enough, which is the case in the Erlenbach when discharge is higher than about 200 $\mathrm{l \cdot s^{-1}}$. Four events

in 2014 ($Q_{\max} \leq 1020\ \mathrm{l \cdot s^{-1}}$) were analysed and the ratio between the measured discharge Q_{meas} and the measured wetted surface A_{wet} derived from the laser measurements are used to determine the mean flow velocity. These measurements showed that the water surface at the measuring section is uneven and asymmetrical (i.e. water table slants across the section). In addition, they indicate that for the discharge range of $300\ \mathrm{l \cdot s^{-1}} < Q < 700\ \mathrm{l \cdot s^{-1}}$ the mean flow velocity is approximatively constant $V_{300<Q<700} \approx 5\ \mathrm{m \cdot s^{-1}}$. Previous estimations of the flow velocity were empirically derived from occasional on-site measurements of the surface velocity (Rickenmann et al. 2014) and have underestimated the mean flow velocity over the geophone cross-section at the Erlenbach.

The mean Froude number was computed as:

$$\mathrm{Fr}_{\mathrm{mean}} = \frac{V_{\mathrm{mean}}}{\sqrt{g \cdot R_{\mathrm{h,mean}}}}\ , \tag{1}$$

where $g = 9.81\ \mathrm{m \cdot s^{-2}}$ is the gravitational acceleration, $V_{\mathrm{mean}} = 5\ \mathrm{m \cdot s^{-1}}$ is the mean flow velocity, $R_{\mathrm{h,mean}} = \frac{A_{\mathrm{wet,mean}}}{P_{\mathrm{wet,mean}}}$ is the mean hydraulic radius, $A_{\mathrm{wet,mean}} = 0.13\ \mathrm{m^2}$ and $P_{\mathrm{wet,mean}} = 1.9$ m are the mean wetted surface and the mean wetted perimeter, respectively. The mean Froude number $\mathrm{Fr}_{\mathrm{mean}}$ at the Erlenbach evaluates at 6.1.

Bedload data

At the Erlenbach the direct bedload measurements were taken with 3 moving basket samplers that were installed in 2008-2009. The baskets have a cubic shape with a side length of 1 m, a volume of 1 $\mathrm{m^3}$ and their mesh has a spacing of 10 mm. The basket samplers are located one meter downstream of the Swiss plate geophones, on the check dam's wall of the sediment retention basin. They are constructed in such a manner that, when activated, they sample all bedload particles transported over the two geophone plates located at the center of the approach flow channel. A complete description of the Erlenbach bedload monitoring site and the automatic basket samplers was given by Rickenmann et al. (2012) who reported: "The devices permit obtaining bedload samples over short sampling periods, determining

the GSD of the transported material and its variation over time and with discharge, and improving the understanding of the geophone signal by providing a direct comparison with the geophone data at short timescales".

The bedload transport detection threshold is based on the impulse rate measured by the Swiss plate geophone. The basket samplers are activated depending on a pre-set discharge range and on a minimum number of geophone impulses. Then, they automatically move into the center of the stream and begin to sample bedload. The sampling time is set to a maximum duration of 10 minutes. To avoid system damage, the maximum mass of the bedload sample is fixed at about 200 kg. The mass of the basket is continuously measured by force sensors in the lower supporting rail, and whenever this threshold-mass is reached the sampler moves out of the measuring section, leading to variable sampling times dependent on the bedload transport rate. Subsequently, the sampled bedload is sieved and the fractions are weighed according to the passing sieve grid sizes (Table 1), with an associated geometric mean size $D_{\mathrm{g,m}}$ for each grain size class. Here we analysed a total of 46 samples which are not exactly identical with those used in the study of Rickenmann et al. (2014), because we were also interested to examine how well the new proposed method also applies to sample masses smaller than about 10 kg.

Swiss plate geophone and signal recording

The Swiss plate geophone consists of a sensor located inside a waterproof housing fixed under the steel plate (Figure 1). The length of the plate in the flow direction is 36 cm, its width 50 cm and its thickness 1.5 cm. The elastomer (an elastic polymer), located between the mounting box and the steel plate, is an important element of the system. It has two main functions: isolate the steel plate from vibrational energy generated in the surroundings and damp the vibrating steel plate. The geophone sensor (GS-20DX manufactured by Geospace Technologies, Houston, Texas) continuously records the vertical oscillations of a steel plate induced by the kinetic impact of a bedload particle (Figure 1).

For a more detailed description of the Swiss plate geophone sensor and the signal it

produces, see Rickenmann et al. (2012), Rickenmann and Fritschi (2010), Wyss et al. (2014) and Rickenmann et al. (2014). When a particle collides against the Swiss plate geophone, some of the energy released by the kinetic impact is transferred to the plate (Turowski et al. 2013). The plate then vibrates and the amplitude of the geophone signal oscillates around the value of zero.

The geophone sensor signal is recorded at a rate $f_s = 10$ kHz for the moving basket sampling periods. Due to this relatively high f_s and the limited storage capacity of the recording system, a few geophone summary values are continuously stored every minute during the normal operation mode of bedload monitoring. The registered values are the number of peaks above a threshold of 0.1 V, termed impulses, the squared integral and the maximum amplitude of the signal. The complete raw signal is recorded over the bedload sampling periods when the basket samplers are activated. It is therefore possible to compute any desired summary values for these periods a posteriori, and then relate them to bedload data derived from the basket sampler.

At the Erlenbach the Swiss plate geophones were installed at the beginning of 2000. Before 2009, the calibration was made through surveys of the sediment volumes deposited in the retention basin. Additional calibration measurements for the sensors were performed using the moving basket samplers from 2009 onwards (Rickenmann et al. 2012).

ANALYSIS OF AMPLITUDE HISTOGRAMS

Computation of packets

Packets can be thought of the complete response of the geophone following a single impact over the Swiss plate geophone. One way to identify the packets is by computing the envelope function of the raw geophone signal (Figure 2). The packet count is analogous to the impulse count, but instead of being computed directly from the raw geophone signal, the number and characteristics of the packets are computed with the help of an envelope function. The crossing of the envelope function with the threshold marks the start and the end of a packet, also defining its duration $\Delta_{t,p}$ (Figure 2). The envelope of the signal is calculated with a Hilbert transform (Jones et al. 2002).

The signal produced by the Swiss plate geophone is not perfectly symmetric and it follows that the envelope's amplitude computed with the Hilbert transform can deviate somewhat from the maxima of the raw signal. However, these deviations are unimportant for our analysis. Indeed, the envelope of the signal is only used to compute the time interval $\Delta_{t,p}$ (Figure 2) for which the maximum amplitude pertaining to a packet is computed from the raw signal.

Impulse and Packet-based amplitude histograms (IbAH and PbAH)

The method developed to extract grain size information is based on the registration of the maximum amplitude of the raw signal within the time-period of an impulse ($\Delta_{t,i}$) and a packet ($\Delta_{t,p}$). The maximum amplitude within these periods is used to assign an impulse or packet to a given amplitude class (AC). The impulse-based amplitude histograms (IbAH) and the packet-based amplitude histograms (PbAH) then represent the number of impulses and packets registered for different AC (Figure 3). The determination of the threshold values to delineate the AC is explained below.

To compute the IbAH and the PbAH, the maximum value of every registered impulse and of the raw signal within a packet (over $\Delta_{t,p}$ in Figure 3) is stored for the same time period that bedload is being collected by the basket samplers. Depending on which is the

198 nearest lower threshold, one impulse (or/and packet) is then attributed to that same AC
199 (Figure 3). The IbAH and PbAH are then calculated by summing the number of impulses
200 and packets registered at those AC ($\boldsymbol{I}$ and $\boldsymbol{P}$ array in Figure 3).

201 **Determining amplitude classes (AC) as a function of grain-size**

202 One key element for the computation of the amplitude histograms are the thresholds at
203 which the impulses and the packets are to be counted. We assume that the relative number
204 of registered impulses or packets between two thresholds is related to the relative fractional
205 bedload mass between the respective sieves (Wyss et al. 2014). The size of the sieves (Table
206 1) are used to compute the respective threshold-amplitudes and therefore the AC at which
207 the impulses and the packets are counted.

208 A relation between the amplitude of the signal and the size of the transported particles is
209 needed for the definition of the threshold amplitudes. For the 46 basket samples, we analyzed
210 the maximum registered amplitude by the geophone MaxA [V] as a function of the B-axis
211 of the largest particle found in the sample $D_{\max}$ [mm] (Figure 4). MaxA can be expressed
212 as a power law function of $D_{\max}$ (Figure 4):

213 $$\mathrm{MaxA} = a_{\mathrm{A}} \cdot D_{\max}^{b_{\mathrm{A}}} , \tag{2}$$

214 where $a_{\mathrm{A}} = 3.56\mathrm{E}^{-4}$, $b_{\mathrm{A}} = 1.75$ and the coefficient of determination $R^2 = 0.74$. This power
215 law fit, as well as all other regression equations presented in this paper were computed with
216 the least-squares solution of the log-transformed data.

217 To compare the measured GSD cumulative curve of the transported bedload samples
218 with the cumulative IbAH/PbAH distribution curve, the distributions are normalized with
219 the average B-axis [mm] of the largest sieved fraction ($D_{\mathrm{g,m_L}}$) and with an estimated average
220 amplitude [V] above the largest defined threshold ($th_{\mathrm{m_L}}$), respectively (Wyss et al. 2014).
221 Wyss et al. (2014) showed that the normalized GSD curve of the transported bedload and
222 the cumulative IbAH/PbAH distribution curve computed from the geophone signal are very

similar (Figure 5).

Assuming a similarity between the relative cumulative GSD and the relative distributions defined by the impulse- and packet amplitude histograms, and using the proportionality defined by equation 2, we obtain:

$$\frac{th_{\mathrm{m}}}{th_{\mathrm{m_L}}} \propto \left(\frac{D_{\mathrm{g,m}}}{D_{\mathrm{g,m_L}}}\right)^{1.75}, \tag{3}$$

where th_{m} is an average amplitude between consecutive threshold-amplitudes defining amplitude classes. The threshold-amplitudes are determined with equation 3 (Table 2) and are then used to compute the amplitude histograms.

Conversion of IbAHD and PbAHD into a GSD

The kinetic impact of a particle on the steel plate results in one packet or in at least one impulse if the amplitude of the signal is large enough to exceed the lowest theshold-amplitude (Table 2). It seems therefore reasonable to use the number of transported particles of each bedload fraction to calibrate the procedure using amplitude histograms. To estimate the number of particles for every grain-size class of the bedload samples, 99 kg of the sieved bedload material from the moving basket samples (sieve sizes accord to Table 1) were taken to manually count the number of particles NG constituting the different fractions. These particle counts were then used to compute the mean mass of a representative particle G_{m} [g] as a function of D [mm] (Table 3 and Figure 6).

A power law function fits well the relation between G_{m} and the mean size of the particles for the fractions larger than $D_{\mathrm{ret}} = 16$ mm (Figure 6):

$$G_{\mathrm{m}} = a_{\mathrm{G}} \cdot D_{\mathrm{g,m}}^{b_{\mathrm{G}}}, \tag{4}$$

where $a_{\mathrm{G}} = 2.19 \cdot 10^{-3}$, $b_{\mathrm{G}} = 2.88$ and $R^2 = 0.999$.

At this point, it is possible to compute the number of particles N constituting each bedload fraction j for each basket sample i:

$$N_{\mathrm{i,j}} = \frac{G_{\mathrm{\_i,j}}}{G_{\mathrm{m\_j}}}, \tag{5}$$

where $G_{\mathrm{i,j}}$ is the mass of the fraction j (ranging from 1 to 7) measured from bedload sample i (ranging from 1 to 46).

Under the assumption that the number of impulses and packets are related to the number of particles, we defined a calibration coefficient α for every fraction j so that:

$$I_{\mathrm{i,j}} = \alpha_{\mathrm{imps\_i,j}} \cdot N_{\mathrm{i,j}}, \text{ and} \tag{6a}$$

$$P_{\mathrm{i,j}} = \alpha_{\mathrm{packets\_i,j}} \cdot N_{\mathrm{i,j}}, \tag{6b}$$

where $I_{\mathrm{i,j}}$ and $P_{\mathrm{i,j}}$ are the number of impulses and packets registered in $\mathrm{AC_j}$ (table 2) from bedload sample i. The α values represent the ratio of number of impulses or packets divided by the estimated number of particles transported over the plate.

We now define a representative α value from the 46 bedload samples for fraction j as:

$$\tilde{\alpha}_{\mathrm{imps\_j}} = \mathrm{median}(\alpha_{\mathrm{imps\_i,j}}), \text{and} \tag{7a}$$

$$\tilde{\alpha}_{\mathrm{packets\_j}} = \mathrm{median}(\alpha_{\mathrm{packets\_i,j}}). \tag{7b}$$

Combining equation 5 with 6a and 6b and with 7a and 7b, the final estimated mass ($G_{\mathrm{est\_IbAH}}$ derived from the IbAH and $G_{\mathrm{est\_PbAH}}$ derived from the PbAH) for the fraction j of the bedload sample i is:

$$G_{\mathrm{est\_IbAH\_i,j}} = \frac{I_{\mathrm{i,j}} \cdot G_{\mathrm{m\_j}}}{\tilde{\alpha}_{\mathrm{imps\_j}}}, \text{ and} \tag{8a}$$

$$G_{\mathrm{est\_PbAH\_i,j}} = \frac{P_{\mathrm{i,j}} \cdot G_{\mathrm{m\_j}}}{\tilde{\alpha}_{\mathrm{packets\_j}}}. \tag{8b}$$

Equations 8a and 8b are used to compute the impulse- and packet-based GSD (GSD_{est_IbAH} and GSD_{est_PbAH}) and are compared to the direct GSD measurements (GSD_{meas}) of the bed-load samples.

RESULTS

Geophone calibration curves

The ratios α of number of impulses or packets divided by the number of particles transported over the plate may be considered as geophone calibration curves, providing α as a function of grain-size for the Erlenbach field measurements. There is a strong increase in the α parameter with particle size, particularly for sizes near the detection limit and up to $D_{\mathrm{g,m}} \approx 17.4$ mm (Figure 7).

For $D_{\mathrm{g,m}} \geq 17.4$ [mm] the relation between $\tilde{\alpha}$ and D is well fitted with a power function:

$$\tilde{\alpha}_{\mathrm{imps_j}} = a_{\mathrm{I}} \cdot D^{b_{\mathrm{I}}} , \text{ and} \tag{9a}$$

$$\tilde{\alpha}_{\mathrm{packets_j}} = a_{\mathrm{P}} \cdot D^{b_{\mathrm{P}}} . \tag{9b}$$

where for $a_{\mathrm{I}} = 0.0122$ and $b_{\mathrm{I}} = 1.09$ equation 9a has a coefficient of determination $R^2 = 0.992$, and for $a_{\mathrm{P}} = 0.0016$ and $b_{\mathrm{P}} = 1.35$, equation 9b has a coefficient of determination $R^2 = 0.996$.

Given the calibrated values of $\tilde{\alpha}$, the estimated weight for every fraction j from event number i was computed with equations 8a and 8b. We first present the computed total bedload fraction mass (the sum of all 46 bedload samples), which are fairly well estimated by both the IbAH and the PbAH (Figures 8a and 8b) in comparison to the measured masses. This is not surprising since the method was calibrated with the measurements.

For each bedload sample i, the estimated GSD ($\mathrm{GSD_{est\_IbAH,i}}$ and $\mathrm{GSD_{est\_PbAH,i}}$) curves are also compared with the measured GSD ($\mathrm{GSD_{meas,i}}$). The ratio r of estimated to measured bedload mass (indicating the relative error) was computed for each grain-size fraction j as:

$$r_{\text{imps\_i,j}} = \frac{G_{\text{est\_IbAH\_i,j}}}{M_{\text{meas\_i,j}}}, \tag{10a}$$

$$r_{\text{packets\_i,j}} = \frac{G_{\text{est\_PbAH\_i,j}}}{M_{\text{meas\_i,j}}}, \tag{10b}$$

$$r_{\text{mean,meas\_i,j}} = \frac{G_{\text{mean,meas\_j}}}{M_{\text{meas\_i,j}}}, \tag{10c}$$

where $G_{\text{mean,meas\_j}}$ stands for an average measured mass for fraction j computed from all basket samples.

The interquartial range IQR of the relative error by the IbAH and the PbAH methods is smaller than 15 % for all fractions (Figure 9a and 9b). Higher relative error values are obtained when simply assuming the averaged measured GSD as a predictor (Figure 9c), in comparison to the errors associated with the IbAHD and PbAHD (Figure 9a and Figure 9b). This clearly shows that the IbAH and the PbAH derived GSD capture quite well changes between different bedload samples.

DISCUSSION

Relation between maximum size of the transported particle and the maximum amplitude of the signal

The field data provide an empirical relation between the maximum amplitude MaxA and the biggest transported particle $D_{\max}$ (Figure 4) registered by the geophone during the calibration measurement. The data in Fig. 4 indicate considerable scatter around the trend of the regression line. The MaxA values may not only depend on particle size or weight mainly because of two additional influencing factors. The first is related to the transport mode: Saltating particles interact less with the stream bed than rolling or sliding particles. They are therefore less likely to impact on the steel plate than rolling ones. The second is associated with the location of the particle impact. It is known from drop tests performed over the Swiss plate geophone that the amplitude of the signal is a function of the impact location over the steel plate (Turowski et al. 2013). Nevertheless, the power relation between MaxA and $D_{\max}$ (Eq. 2) was used to define appropriate amplitude ranges for the histogram method. One may expect that some of the perturbating factors (rotation of particle, angle, velocity and location of impact) may average out for large observation periods.

Particle-size detection limit

From laboratory experiments it is known that turbulent flow over the Swiss plate geophone induces low frequency vibrations which contribute to background noise. To have a clear distinction between the signal and the noise, the lowest defined threshold-amplitude for the impulse detection should be larger than the amplitude of the background noise level A_{noise}. The geophone produces a zero mean signal and therefore A_{noise} can be estimated by its standard deviation for the time periods when no impacts (or signal peaks) are detected. A_{noise} was determined as 0.005 V for the sample period with the highest recorded discharge $Q = 1321\,\text{l}\cdot\text{s}^{-1}$ for which the complete raw signal was registered.

Our method implies that smaller particles can potentially be detected if the lowest threshold amplitude for the impulse/packet count is lowered. The empirical relation between the

maximum registered amplitude and the size of the largest transported particle (Figure 4 and equation 2) indicates that the particle size corresponding to A_{noise} is about 6 mm. This is an estimate of the particle-size detection limit for a simple (i.e. without any kind of signal pre-processing or filtering) amplitude-based method from the raw signal for the Swiss plate geophone at the Erlenbach.

Overlapping probability of multiple packets (impact signals)

Before bedload is sampled by the basket samplers, it is transported over two central geophone plates (gp_{left} and gp_{right}) installed in the measuring cross-section. Due to asymmetrical flow conditions, most of the sampled bedload (about 80 %) travels over the orographic right side of the cross-section (Rickenmann and McArdell 2007). Consequently, more impulses and packets are recorded by gp_{right} than by gp_{left}.

Counting the packets individually is only possible if no overlap exists between them. An overlapping probability indicator is the ratio z_{p} of the summed durations of packets, $\sum \Delta_{\text{t,p}}$, to the whole sampling time $\Delta_{\text{t,sample\_i}}$. We analysed this ratio for the two geophone plates (gp_{left} and gp_{right}) over which bedload is transported for the 46 bedload samples:

$$z_{\text{p,left/right}} = \frac{\sum \Delta_{\text{t,p,left/right}} \text{ of sample i}}{\Delta_{\text{t,sample\_i}}}. \tag{11}$$

The z_{p} ratio is typically within the range 10^{-5} to 10^{-2} (Figure 10). Only in some extreme cases (5 out of the 46 samples), the total duration of the packets accounts for more than 1 % of the whole sampling time. This means that for most of the samples, the summed duration of the packets is at least two order of magnitudes smaller than the total sampling time, and it is therefore unlikely for packets to overlap. Given that z_{p} is also a measure of transport activity, total unit bedload transport rate q_{s} $[\text{kg} \cdot \text{m}^{-1}\text{s}^{-1}]$ for each bedload sample can be partitioned into two bedload transport rates, one corresponding to bedload transported over gp_{left} ($q_{\text{s,lef}}$) and the other over gp_{right} ($q_{\text{s,right}}$) as follows:

$$q_{\mathrm{s,left}} = 2\,\frac{z_{\mathrm{p,left}}}{z_{\mathrm{p,left}} + z_{\mathrm{p,right}}}\,q_s, \tag{12a}$$

$$q_{\mathrm{s,right}} = 2\,\frac{z_{\mathrm{p,right}}}{z_{\mathrm{p,left}} + z_{\mathrm{p,right}}}\,q_s, \tag{12b}$$

where $z_{\mathrm{p,left}}$ and $z_{\mathrm{p,right}}$ is the packet overlapping probability z_{p} recorded by $\mathrm{gp_{left}}$ and $\mathrm{gp_{right}}$, respectively. The factor 2 is due to the unit solid discharge calculation for each plate with the width $b = 0.5$ m: $(Q_{\mathrm{s}}/b) = (Q_{\mathrm{s}}/0.5\ \mathrm{m}) = 2 \cdot q\mathrm{s}$, where Q_{s} is the total solid discharge over the two plates.

Packet overlapping probability $z_{\mathrm{p,left/right}}$ increases almost linearly with increasing unit bedload transport rate for each plate (Figure 10):

$$z_{\mathrm{p,left}} = a_{\mathrm{left}} \cdot q_{\mathrm{s,left}}^{b_{\mathrm{left}}}\,, \tag{13a}$$

$$z_{\mathrm{p,right}} = a_{\mathrm{right}} \cdot q_{\mathrm{s,right}}^{b_{\mathrm{right}}}\,, \tag{13b}$$

where $a_{\mathrm{left}} = 0.0152$ and $b_{\mathrm{left}} = 0.97$ equation 13a has a coefficient of determination $R^2 = 0.98$, and for $a_{\mathrm{right}} = 0.0154$ and $b_{\mathrm{right}} = 0.96$, equation 13b has a coefficient of determination $R^2 = 0.97$. A z_{p} value of 1 indicates the theoretical limit for the detection of all packets. For the large events at the Erlenbach ($Q \geq 3\ \mathrm{m^3 \cdot s^{-1}}$) the measured unit bedload transport rates have been reported to be larger than about 100 $\mathrm{kg \cdot m^{-1} \cdot s^{-1}}$ (Hegg and Rickenmann 1999). For such intensive transport rates, the value of z_{p} is expected to be close to 1 (Figure 10) and thus the number of identified packets from the geophone signal with the presented method may not deliver accurate measurements of bedload transport rates.

Number of registered impulses or packets per particle α

There is an increase in α with particle size (Figure 7). The number and size of registered impulses by the Swiss plate geophone depend on (Etter 1996; Rickenmann et al. 2012;

Turowski and Rickenmann 2009; Turowski et al. 2013):

- (A): The impact location on the plate,
- (B): the energy of the particle impact transmitted to the plate,
- (C): the mode of transport and particle shape and
- (D): the number of particle impacts for a given size.

The swiss plate geophone reacts symmetrically (Turowski et al. 2013). Assuming that a bedload particle is equally likely to impact at each point over the plate, one could attribute a mean number of registered impulses for a given particle and the effect of the impact location on the plate (A) would be averaged. The use of amplitude histograms implicitly accounts for the grain-size dependent part of the impact energy (B). Particle shape, i.e. its sphericity and roundness (C), has an effect on transport mode (Etter 1996; Krein et al. 2008). However, it has been reported that mainly transport mode rather than the symmetry of the particles sets the number of impulses registered by the Swiss plate geophone (Turowski and Rickenmann 2009). The increase of the proportionality coefficient α (Figure 7) with particle size could be explained mainly with an increase in the number of particle impacts with increasing particle size (D). Indeed, saltation is dominated by drag forces (van Rijn 1984). Saltation transport mode probability is therefore higher for smaller particles. From field observations in a gravel bed stream, Drake et al. (1988) reported that large bedload particles underwent displacement by rolling, whereas smaller particles underwent displacement by saltation. Rolling particles involve more particle-bed interaction (Lajeunesse et al. 2010), and in our case more impacts against the Swiss plate geophone and therefore more impulses are registered by the geophone on average for larger compared to smaller particles.

Swiss plate geophone calibration improvement

The Swiss plate plate geophone has been previously calibrated for total transported mass with an impulse-based method at the Erlenbach. Rickenmann et al. (2012) related the number of impulses registered above a threshold value of 0.1 V ($IP_{0.1\mathrm{V}}$) to 27 bedload

samples ($D > 9.5$ mm) caught by the basket samplers for the period 2009 and 2010. A linear calibration coefficient k_b between the total number of impulses and the measured transported bedload mass was suggested:

$$IP_{0.1\mathrm{V}} = k_\mathrm{b} \cdot G_\mathrm{meas,b}, \tag{14}$$

where k_b has a value of 3.27 kg^{-1} for the period 2009-2010 and $G_\mathrm{meas,b}$ is the total sampled bedload material ($D > 9.5$ mm). A similar calibration was obtained for a total of 46 samples covering the period 2009 to 2012 (Rickenmann et al. 2014).

To compare this earlier calibration approach ($IP_{0.1\mathrm{V}}$) to the IbAH- and PbAH methods, we calculated $G_\mathrm{meas,b}$ for the same bedload samples as analysed in this study (46 basket samples for the period 2010-2012) as a function of $IP_{0.1\mathrm{V}}$:

$$G_\mathrm{meas,b} = C_\mathrm{IP} \cdot IP_{0.1\mathrm{V}}, R^2 = 0.97, \tag{15}$$

where $C_\mathrm{IP} = 0.29$ is valid for total mass estimates with $D > 9.5$ mm.

For the three methods, the linear regressions between $G_\mathrm{meas,b}$ and the computed bedload masses (G_comp) for all 46 basket samples (Figure 11) indicate the degree of agreement:

$$G_{\mathrm{comp},\,C_\mathrm{IP}} = 0.97 \cdot G_\mathrm{meas,b},\ R^2 = 0.97,\ s_\mathrm{e} = 0.143,\ s_\mathrm{e,log} = 0.072, \tag{16a}$$

$$G_{\mathrm{comp},\,\mathrm{IbAH}} = 0.98 \cdot G_\mathrm{meas,b},\ R^2 = 0.99,\ s_\mathrm{e} = 0.146,\ s_\mathrm{e,log} = 0.080, \tag{16b}$$

$$G_{\mathrm{comp},\,\mathrm{PbAH}} = 1.02 \cdot G_\mathrm{meas,b},\ R^2 = 0.99,\ s_\mathrm{e} = 0.143,\ s_\mathrm{e,log} = 0.071, \tag{16c}$$

where s_e is the relative standard error of the computed bedload masses and $s_\mathrm{e,log}$ is the relative standard error calculated with the log-tranformed computed bedload masses.

Remark on fitted functional relationships

Note that the regression equations for the mean particle number (Eq. 4) and for the calibration coefficients alpha (Eq. 9a and 9b) were not directly used here for the computation of the quantitative results, because for each grain size fraction directly measured values were available. These regression equations are presented for illustrative purposes, and they would allow an estimation of transported bedload masses also for differently defined grain size fractions. The reason for having fitted the power equations (equations 9a and 9b) is because we consider that the number of registered impulses/packets at different amplitude-thresholds α may be a good parameter to compare a field-based with flume-based calibration. The fitted equation describing how the mean particle weight G_{m} increases with particle size D (equation 4) could also be used to explain the different geophone response and therefore geophone calibration between different field sites.

Particle counting

For six bedload- and bed-material samples from mountain gravel-bed rivers, Bunte and Abt (2001) analysed the mean mass per particle G_{m} [g] as a function of the retaining sieve size D_{ret} in [mm]. Their results suggested a general power law function in the form of:

$$G_{\mathrm{m}} = a \cdot D_{\mathrm{ret}}^{b}. \tag{17}$$

The values of the coefficient a obtained by Bunte and Abt (2001) are slightly larger than the one computed from the particle count at the Erlenbach (Table 4).

A comparison of G_{m} between different field sites is of interest, because it affects the α-values. The variability of the coefficient a and the exponent b in Table 4 shows that even for streams of the same petrology, the number of particles can vary for that same size fraction. If we can isolate this effect on the α-values, this will help explaining other factors affecting geophone calibration in different streams, e.g. particle shape and/or hydraulic conditions.

Notice that for the Erlenbach, $\min(D_{\mathrm{ret}}) = 16$ mm was chosen to fit Eq. 17 (Table

4) instead of the smallest used sieve with a grid spacing of 9.5 mm (Table 1), because the smallest sieved grain-size fraction at the Erlenbach (i.e. 9.5 and 16 mm sieves), is considerably larger than the equivalent grain-size fraction (11.3 and 16 mm sieves) in Bunte and Abt (2001).

About the implementation of the IbAH and the PbAH methods

It is possible to store the full raw signal, but it is inconvenient to do this at all times due to the limited digital storage capacity at field monitoring stations. For continuous measurements, a tradeoff between the computation of signal summary values and their relevance for calibration implementation has therefore to be done. The main advantage of the IbAH over the PbAH approach is its easy technical implementation. The algorithm for computing the number of impulses is simple and it allows to continuously register the number of impulses and the related IbAH for real-time data acquisition in the field and efficient storage. The computation of the packets for the PbAH method is clearly more processor-demanding. Its implementation for continuous bedload monitoring in the field has to be tested yet.

CONCLUSIONS AND OUTLOOK

We presented the calibration coefficient α as the relative number of registered impulses or packets (representing a single particle impact) per transported particle and for a given amplitude class. The calculation of this value is based on an analysis of the raw signal of the Swiss plate geophone measuring system. The accuracy of the calibrated fractional bedload mass estimation by the impulse-based amplitude histogram (IbAH) and the packet-based amplitude histogram (PbAH) is around 10 % for most of the analysed bedload samples. Our results show that the use of amplitude histograms, a metric describing the statistical distribution of the signal's amplitude, allows to continuously extract GSD information during measurements with impact plate geophones. Such measurements are suitable for a better understanding of bedload transport processes in steep streams.

Systematic flume experiments within the expected flow velocity range observed in the field and using natural bedload particles from that same site are under way. Applying the method presented here, these experiments will demonstrate if it is possible to derive a flume-based calibration relation for the Swiss plate geophone.

Etter (1996) showed that the median frequency of the Swiss plate geophone (at the time with a piezoelectrical sensor as transducer) decreases somewhat linearly with particle size which corresponds well with previous observations made by Thorne (1986). Although the simple amplitude-based approach to extract GSD information from the Swiss plate geophone signal produces fairly good GSD estimations for the Erlenbach stream, its accuracy might increase when taking frequency information of the signal into account.

ACKNOWLEDGEMENTS

This study was supported by the Swiss National Science Foundation SNSF, grant 200021_137681. We thank numerous WSL colleagues for their support with fieldwork at the Erlenbach.

REFERENCES

Badoux, A., Andres, N., and Turowski, J. M. (2014). "Damage costs due to bedload transport processes in Switzerland." *Natural Hazards and Earth System Science*, 14, 279–294.

Bänziger, R. and Burch, H. (1990). "Acoustic sensors (hydrophones) as indicators for bedload transport in a mountain torrent." *Hydrology in Mountainous Regions I*, Vol. IAHS Publication 193, International Association of Hydrological Sciences, Wallingford, 207–214.

Barrière, J., krein, A., Oth, A., and Schenkluhn, R. (2014). "Characterizing bedload transport using its acoustic fingerprint: from total power to signal time-frequency attributes." Submitted. *Earth Surf. Process. Landforms.*

Beer, A. R., Turowski, J. M., Fritschi, B., and Rieke-Zapp, D. H. (2014). "Field instrumentation for high-resolution parallel monitoring of bedrock erosion and bedload transport." Accepted. *Earth Surf. Process. Landforms.* DOI: 10.1002/esp.3652.

Belleudy, P., Valette, A., and Graff, B. (2010). "Passive hydrophone monitoring of bedload in river beds: First trials of signal spectral analyses." *Scientific Investigations Report 5091.*

Bogen, J. and Møen, K. (2003). "Bed load measurements with a new passive acoustic sensor." *Erosion and Sediment Transport Measurement in Rivers: Trends and Explanation (Proceedings of the Oslo Workshop, June 2002)*, J. Bogen, T. Fergus, and D. E. Walling, eds., Vol. 283 of *IAHS Publication*, IAHS, 181–182.

Bunte, K. (1996). "Analyses of the temporal variation of coarse bedload transport an its grain size distribution." *Report RM-GTR-288*, United States Department of Agriculture (December).

Bunte, K. and Abt, S. R. (2001). "Sampling surface and subsurface particle-size distributions in wadable gravel- and cobble-bed streams for analyses in sediment transport, hydraulics, and streambed monitoring." *Report RMRS-GTR-74*, United States Department of Agriculture (May).

Drake, T. G., Shreve, R. L., Dietrich, W. E., Whiting, P. J., and b. Leopold, L. (1988). "Bedload transport of fine gravel observed by motion-picture photography." *J. Fluid Mech.*, 192,

193–217.

Etter, M. (1996). "Zur Erfassung des Geschiebetransportes mit Hydrophonen." *Diploma Thesis.* University of Berne and WSL, 110pp.

Geay, T. (2013). "Mesure acoustique passive du transport par charriage dans les rivières." *PhD Thesis.*

Gray, J. R., Laronne, J. B., and Marr, J. D. (2010). "Bedload-surrogate monitoring technologies." *U.S. Geological Survey Scientific Investigations Report 5091*, (http://pubs.usgs.gov/sir/2010/5091/).

Hegg, C. and Rickenmann, D. (1999). "Comparison of bedload transport in a steep mountain torrent with a bedload transport formula." *Hydraulic Engineering for Sustainable Water Resources Management at the Turn of the Millenium*, IAHR.

Jones, E., Oliphant, T., Peterson, P., et al. (1999-2002). "SciPy: Open source scientific tools for Python, <http://www.scipy.org/>. [Online; accessed 08.07.2014].

Krein, A., Klinck, H., Eiden, M., Symader, W., Bierl, R., Hoffmann, L., and Pfister, L. (2008). "Investigating the transport dynamics and the properties of bedload material with a hydro-acoustic measuring system." *Earth Surf. Process. Landforms*, 33, 152–163.

Lajeunesse, E., Malverti, L., and Charru, F. (2010). "Bed load transport in turbulent flow at the grain scale: Experiments and modeling." *J. Geophys. Res.*, 115, F04001.

Møen, K. M., Bogen, B. J., Zuta, J. F., Ade, P. K., and Esbensen, K. (2010). "Bedload measurement in rivers using passive acoustic sensors." *U.S. Geological Survey Scientific Investigations Report 5091*, (http://pubs.usgs.gov/sir/2010/5091/).

Rickenmann, D. (1997). "Sediment transport in Swiss torrents." *Earth Surf. Process. Landforms*, 22, 937–951.

Rickenmann, D. (2012). "Alluvial steep channels: Flow resistance, bedload transport prediction, and transition to debris flows." *Gravel Bed Rivers: Processes, tools, environments*, M. Church, P. Biron, and A. Roy, eds., John Wiley and Sons, Chapter 28, 386–397.

Rickenmann, D. and Fritschi, B. (2010). "Bedload transport measurements using piezoelec-

tric impact sensors and geophones." *U.S. Geological Survey Scientific Investigations Report 5091*, (http://pubs.usgs.gov/sir/2010/5091/).

Rickenmann, D. and McArdell, B. W. (2007). "Continuous measurement of sediment transport in the Erlenbach stream using piezoelectric bedload impact sensors." *Earth Surf. Process. Landforms*, 32, 1362–1378.

Rickenmann, D., Turowski, J. M., Fritschi, B., Klaiber, A., and Ludwig, A. (2012). "Bedload transport measurements at the Erlenbach stream with geophones and automated basket samplers." *Earth Surf. Process. Landforms*, 37, 1000–1011.

Rickenmann, D., Turowski, J. M., Fritschi, B., Wyss, C. R., Laronne, J., Barzilai, R., Reid, I., Kreisler, A., Aigner, J., Seitz, H., and Habersack, H. (2014). "Bedload transport measurements with impact plate geophones: comparison of sensor calibration in different gravel-bed streams." *Earth Surf. Process. Landforms*, 39, 928–942.

Schuerch, P., Densmore, A. L., McArdell, B. W., and Molnar, P. (2006). "The influence of landsliding on sediment supply and channel change in a steep mountain catchment." *Geomorphology*, 78, 222–235.

SICK (2014). "Laserscanner TiM5xx/TiM55x/Outdoor/Short Range, <http://www.sick.com>. [Online; accessed 23.09.2014].

Thorne, P. D. (1986). "Laboratory and marine measurements on the acoustic detection of sediment transport." *J. Acoust. Soc. Am.*, 80(3), 899–910.

Turowski, J. M., Böckli, M., Rickenmann, D., and Beer, A. (2013). "Field measurements of the energy delivered to the channel bed by moving bed load and links to bedrock erosion." *J. Geophys. Res. Earth Surf.*, 118, 2438-2450.

Turowski, J. M. and Rickenmann, D. (2009). "Tools and cover effects in bedload transport observations in the Pitzbach, Austria." *Earth Surf. Process. Landforms*, 34, 26–37.

Turowski, J. M. and Rickenmann, D. (2011). "Measuring the statistics of bedload transport using indirect sensors." *J. Hydr. Eng.*, 137(1), 116–121.

van Rijn, L. C. (1984). "Sediment transport, part i: bed load transport." *J. Hydr. Eng.*, 110,

1431–1456.

Wyss, C. R., Rickenmann, D., Fritschi, B., Turowski, J. M., Weitbrecht, V., and Boes, R. M. (2014). "Bedload grain size estimation from the indirect monitoring of bedload transport with Swiss plate geophones at the Erlenbach stream." *Proc. Int. Riverflow Conference*, 1907–1912.

List of Tables

TABLE 1. Grid sizes used at the Erlenbach for sieving, bedload fractions fractions and associated $D_{\mathrm{g,m}}$.

fraction [-]	retaining sieve D_{ret} [mm]	passing sieve D_{pass} [mm]	$D_{\mathrm{g,m}}$ [mm]
1	9.5	16	12.3
2	16	19	17.4
3	19	25	21.8
4	25	31.5	28.1
5	31.5	45	37.6
6	45	63	53.2
7	63	–	83 *

* The geometric mean size of the largest bedload fraction was calculated from 626 individually measured particles which were retained by the largest sieve for all 46 bedload samples.

TABLE 2. Amplitude classes and amplitude thresholds used for the computation of amplitude histograms; corresponding mean particle size is listed as well.

AC # [-]	lower threshold [V]	upper threshold [V]	th_{m} [V]	$D_{\mathrm{g,m}}$ [mm]
1	0.0176	0.0438	0.0307	12.3
2	0.0438	0.0590	0.0514	17.4
3	0.0590	0.0955	0.0773	21.8
4	0.0955	0.1432	0.1196	28.1
5	0.1432	0.2675	0.2054	37.6
6	0.2672	0.4815	0.3744	53.2
7	0.4815	–	0.81 (estim.)	83

TABLE 3. Number of particles $NG_{\text{-j}}$ constituting the weighed fraction j (G) at the Erlenbach.

fraction	#	1	2	3	4	5	6	7	
$D_{\text{g,m}}$	[mm]	12.3	17.4	21.8	28.1	37.6	53.2	86	
G	[kg]	22.1	12.6	12.1	7.1	7	4.5	33.3	$\sum = 99$
NG	[-]	24698	1482	742	219	100	23	42	$\sum = 27306$
G_{m}	[g]	0.9	8.5	16.3	32.2	69.8	197.3	792.6	

TABLE 4. Coefficient a and exponent b computed with Eq. 17 for two geologically distinct stream petrologies.

	$\min(D_{\mathrm{ret}})$ [mm]	petrology	a	b	R^2 [-]
Bunte and Abt (2001) for six gravel-bed rivers	11.3	granitic and andesite	0.0024−0.0036	2.92−3.04	0.999
Erlenbach (this study)	16	flysch (Rickenmann 2012)	0.0022	3.0	0.998

List of Figures

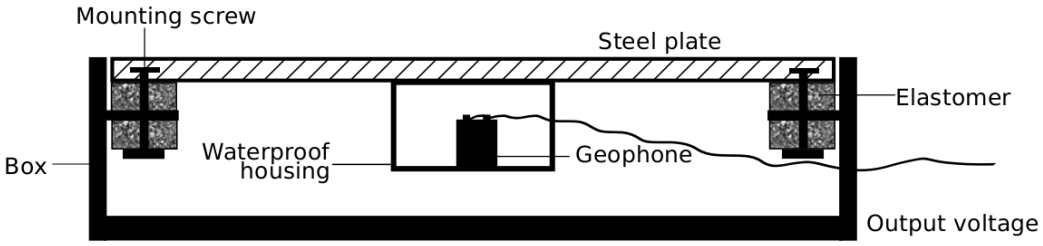

FIG. 1. Schematic cross-section of the Swiss plate geophone.

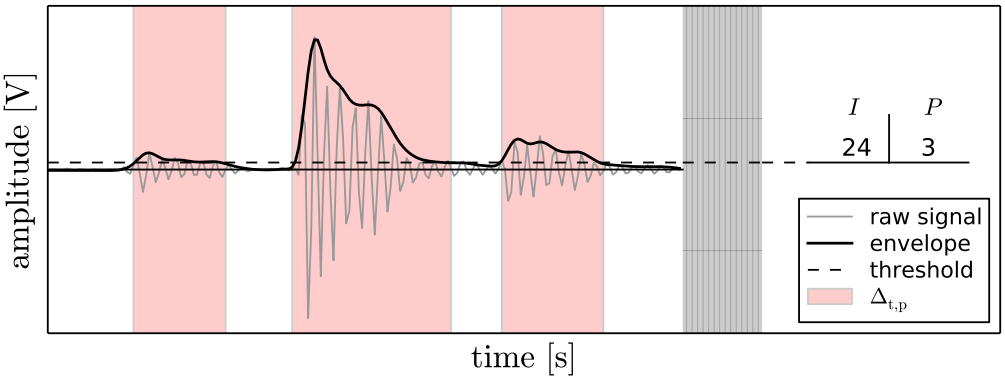

FIG. 2. Computation of number of impulses ($I = 24$) and packets ($P = 3$) registered over a unique threshold-amplitude. This Figure illustrates an example of how an impulse is counted every time that the raw signal exceeds a pre-defined threshold and how $\Delta_{t,p}$ is defined by the crossing of the envelope with that same threshold.

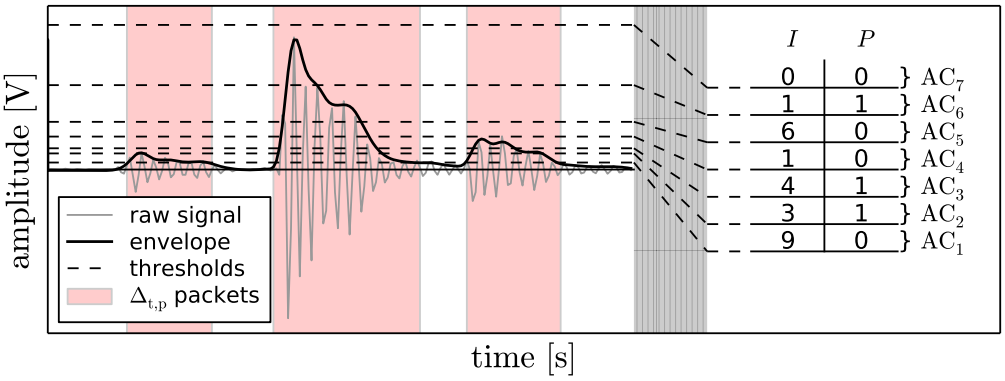

FIG. 3. IbAH (I-array) and PbAH (P-array) computed from the raw signal registered during a real bedload transport event at the Erlenbach. This example illustrates how the number of impulses and packets are summed up at different AC to create the amplitude histograms.

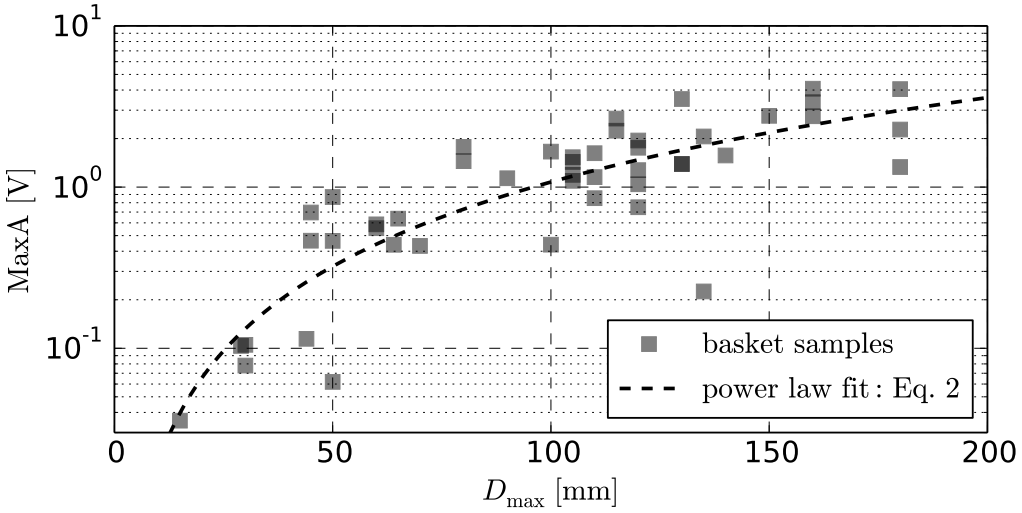

FIG. 4. MaxA **vs** $D_{\max}$ **for the** 46 **bedload samples fitted with Eq. 2.**

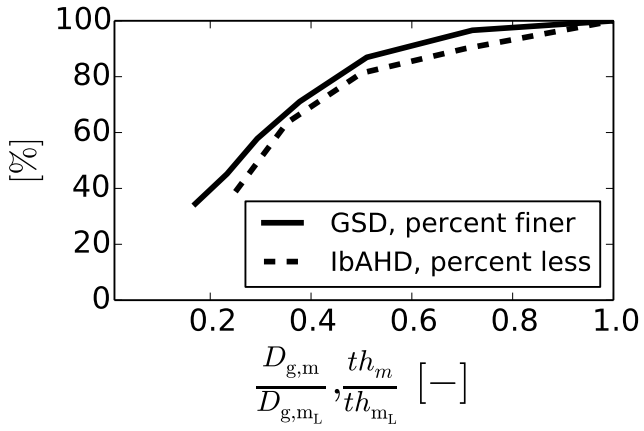

FIG. 5. Example of normalized GSD and IbAHD curves for a bedload sample taken during a flood event on the 17th July 2010. D_{m} **and** th_{m} **are normalized with** $D_{\mathrm{g,m_L}}$ **and** $th_{\mathrm{m_L}}$**, respectively.**

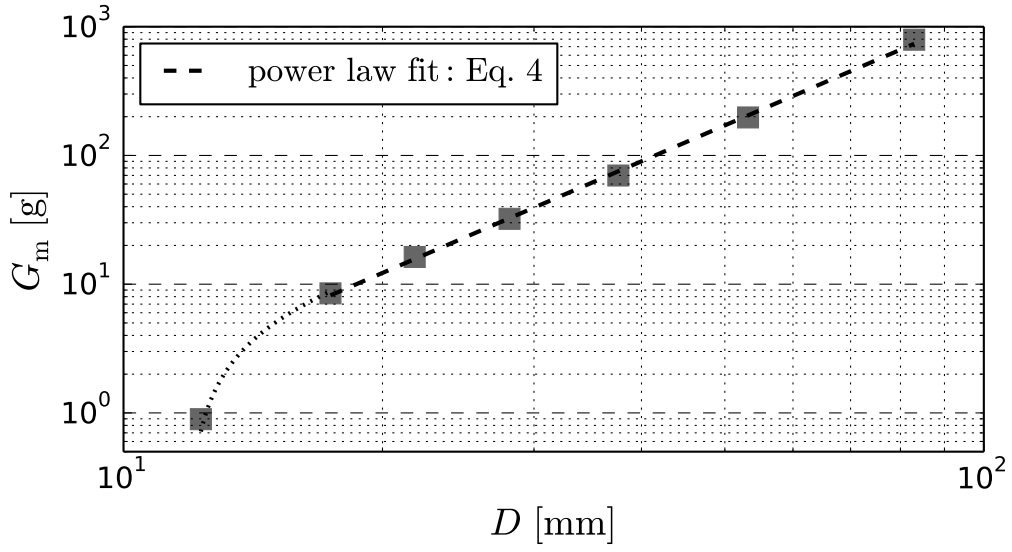

FIG. 6. Mean particle mass G_m as a function of particle size D. For $D_\mathrm{g,m} \geq 17.4$ mm the data is well fitted with a power law function (Eq. 4).

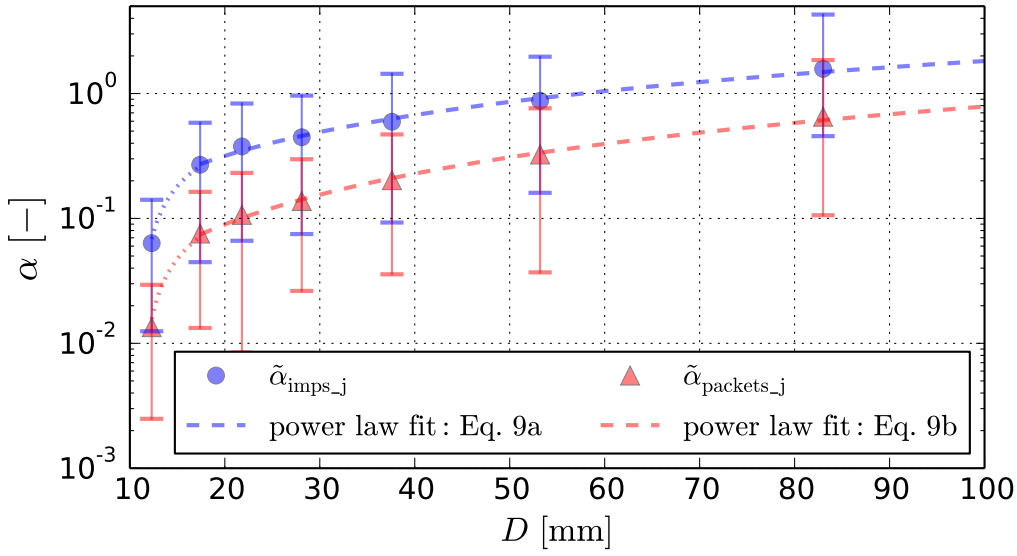

FIG. 7. Calibrated ratios $\tilde{\alpha}$ (representing a relative number of impulses or packets divided by the number of transported particles) and its interquartile range (IQR) as a function of D. A power law function fits well the relation for the bigger fractions $D_{\text{g,m}} \geq 17.4$ mm (Eq. 9a and 9b).

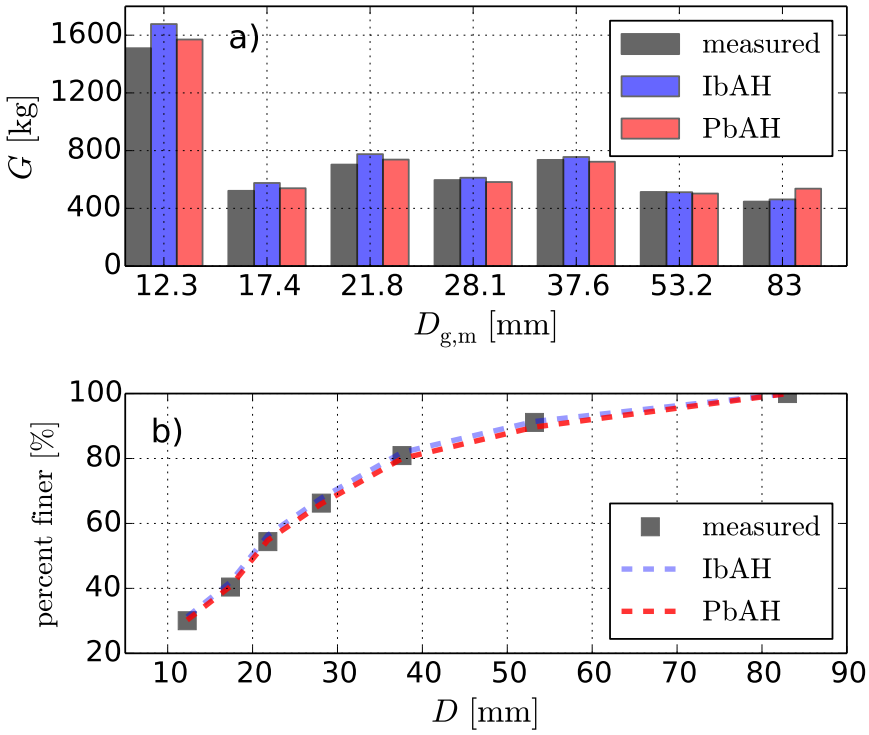

FIG. 8. a) Measured and estimated fraction mass for the sum of all 46 bedload samples. b) respective cumulative distribution curves.

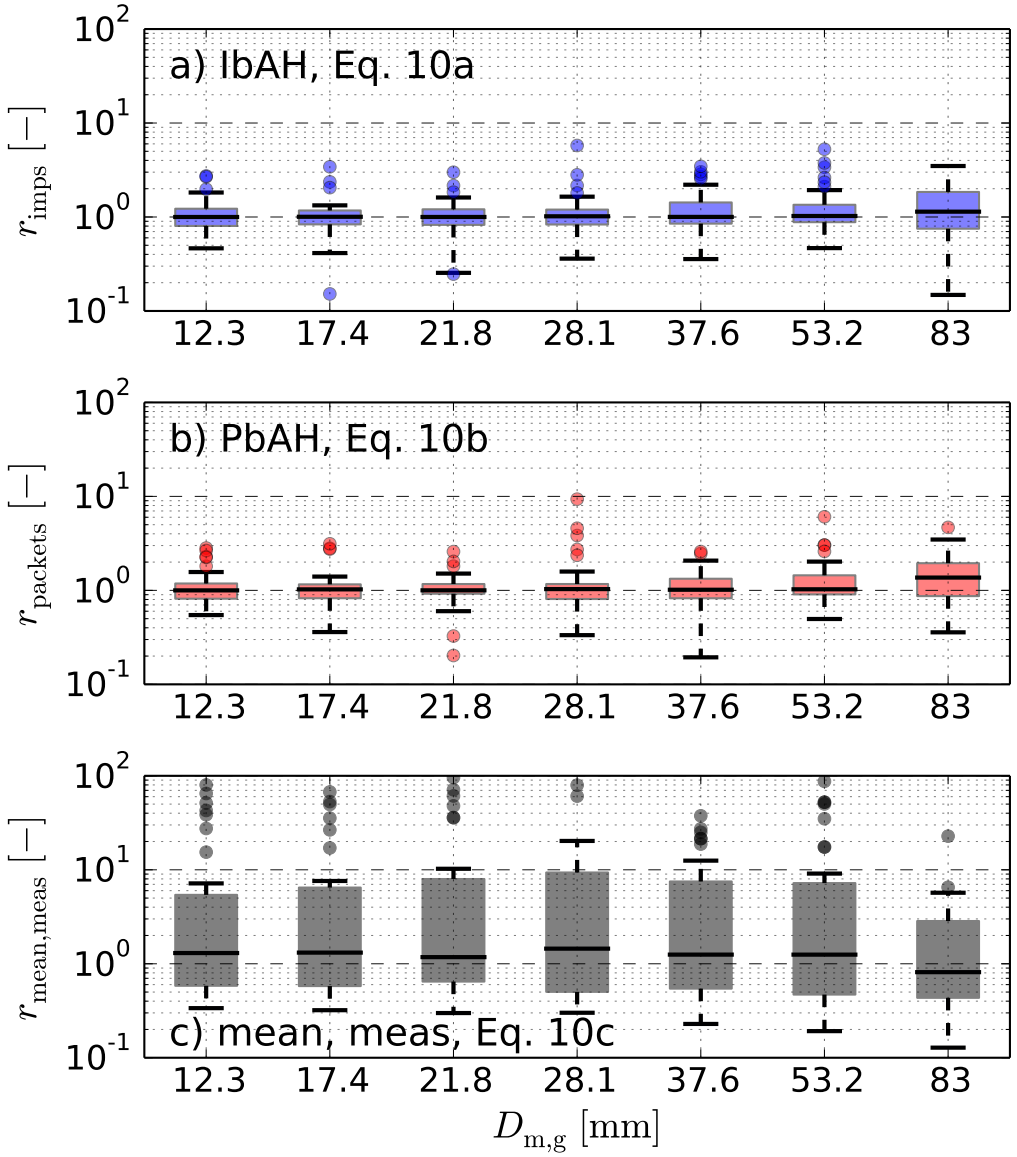

FIG. 9. Ratio r between the measured bedload fraction mass and the on estimated with a) the IbAH method, b) the PbAH method and c) the averaged measured fraction mass of all bedload samples computed with equations 10a, 10b and 10c respectively.

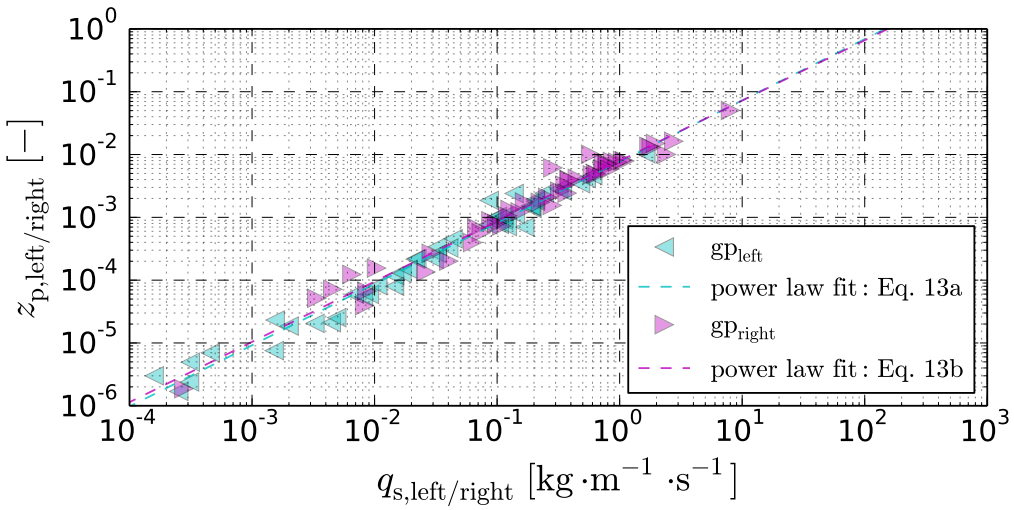

FIG. 10. z_{p} **ratio of the left and the right central geophone plates (**$\mathrm{gp}_{\mathrm{left}}$ **and** $\mathrm{gp}_{\mathrm{right}}$**) as a function of unit bedload transport rate.**

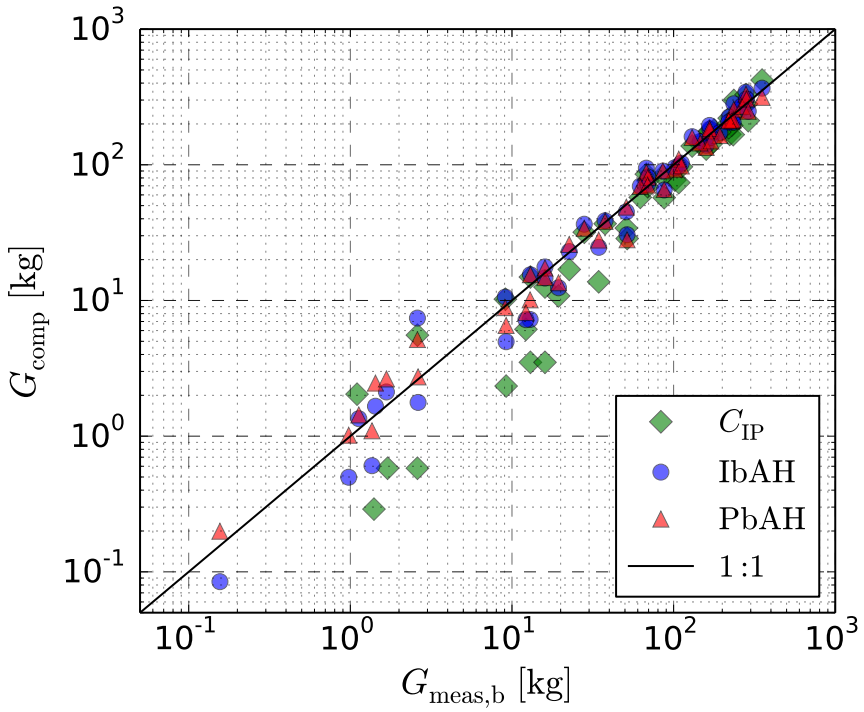

FIG. 11. Computed vs measured bedload mass for the impulse-based calibration (C_{IP}), the IbAH and the PbAH calibration methods.